CHINA FOUNDRY Research & Development
Vol. 23 No. 2 March 2026
www.springer.com/41230
https://doi.org/10.1007/s41230-026-5118-1

# Effect of grain size on fatigue behaviors of Mg-2.6Nd-0.35Zn-*x*Zr alloys

**Lun-yong Zhang[1, 2], Yan-ping Chen[1, 2], Xian-xing Wang[1, 2], Hong-xian Shen[1, 2], *Hong-hui Liu[3, 4], **Fu-yang Cao[1, 2], ***Zhi-liang Ning[1, 2], and ****Jian-fei Sun[1, 2]**

*1. School of Materials Science and Engineering, Harbin Institute of Technology, Harbin 150001, China*

*2. National Key Laboratory of Precision Hot Processing of Metals, Harbin Institute of Technology, Harbin 150001, China*

*3. Qinghai Institute of Salt Lakes, Chinese Academy of Sciences, Xining 810008, China*

*4. Institute of Metal Research, Chinese Academy of Sciences, Shenyang 110016, China*



**Abstract:** High-performance magnesium alloys are in great demand to meet the lightweight design requirements of aircraft. Grain size has long been recognized as a key factor influencing the mechanical properties of alloys. This study investigates the effect of grain size, controlled by Zr addition, on the fatigue behavior of a recently developed low-cost Mg-2.6Nd-0.35Zn alloy, through systematic characterization and analysis of stress-life (*S-N*) curves, fatigue crack propagation, fracture surface morphology, stress intensity factor, and crack propagation threshold. The results show that after heat treatment (solution at 525±5 °C for 8 h and water quenching at 60–80 °C, followed by aging at 250±5 °C for 14 h and then air cooling), coarse-grained specimens (average grain size approximately 596 μm) containing 0.12wt.% Zr exhibit greater resistance to fatigue crack propagation than fine-grained specimens (average grain size approximately 94 μm) containing 0.46wt.% Zr. Coarse grains promote intergranular fracture, while fine grains favor transgranular fracture. In addition, coarse grains reduce the sensitivity of the crack tip to stress concentration. Furthermore, fine-grained samples demonstrate a longer total fatigue life, owing to their superior resistance to crack initiation, which significantly prolongs the crack initiation stage. These findings highlight the importance of optimizing grain size to achieve the best possible fatigue resistance in Mg-Nd-Zn-Zr alloys for practical engineering applications.

**Keywords:** Mg-Nd-Zn-Zr alloys; grain size; fatigue behaviors; crack propagation; crack initiation

**CLC numbers:** TG146.22 **Document code:** A **Article ID:** 1672-6421(2026)02-186-11

## 1 Introduction

Magnesium alloys have been widely adopted in fields such as aerospace, automotive engineering, and biomedical devices owing to their lightweight nature, favorable mechanical properties, and good biocompatibility[1-3]. Recently, a low-cost magnesium alloy family with composition of Mg-Nd-Zn-Zr was developed to overcome the poor ductility and low strength limit of conventional magnesium alloys[4, 5]. This new family of alloys exhibit high strength and excellent biological performance, showing great potential for a variety of applications. Considerable efforts thus have been devoted to investigate the effects of various factors on the mechanical properties of this emerging magnesium alloy family[6, 7].

It has been reported that increasing the cooling rate in the range of 0.4–2.4 °C·s$^{-1}$ for an as-cast Mg-Nd-Zn-Zr alloy can reduce the grain size from 66 to 44 μm while increasing the volume fraction of eutectic compounds ($Mg_{12}Nd$) from 3% to 6.1%. This change leads to a complex modulation of mechanical properties, as a smaller grain size generally enhances yield strength, ultimate tensile strength, and elongation. However, $Mg_{12}Nd$ primarily deteriorates yield strength and ultimate tensile strength[8]. By adjusting the

***Hong-hui Liu**

Ph. D., Professor. His research interests primarily focus on materials development and casting technologies of magnesium and aluminum alloys.

E-mail: liuhh@isl.ac.cn

****Fu-yang Cao**

E-mail: caofuyang@hit.edu.cn

*****Zhi-liang Ning**

E-mail: zhiliangning@sina.com

******Jian-fei Sun**

E-mail: jfsun_hit@263.net

**Received: 2025-05-27; Revised: 2025-07-07; Accepted: 2025-09-16**

Nd, Zn, and Zr contents, the hardness and yield strength of Mg-Nd-Zn-Zr alloys have been shown to be influenced by both the average grain size (determined by Zr content) and the concentration of Nd and Zn[9]. Grain refinement strengthening is therefore critical for improving the mechanical performance of Mg-Nd-Zn-Zr alloys, a strategy also validated in other magnesium alloy families, where it is often achieved by adding the grain refiner Zr[10, 11]. Li et al.[12] systematically studied the effect of grain size on the tensile properties of Mg-3Nd-0.2Zn-*x*Zr. They reported that both yield strength and ultimate tensile strength increased with decreasing grain size, particularly after aging. Additionally, heat treatment conditions significantly influenced the relationship between grain size ($d$) and mechanical properties. Under T4 heat treatment, the Hall-Petch strength coefficients were 9.1±0.42 MPa·mm$^{1/2}$ for $d$ =43–172 μm ($x$=0.05–0.5) and 21.7±0.74 MPa·mm$^{1/2}$ for $d$ =172–1,526 μm ($x$=0–0.05). After T6 treatment, these coefficients increased to 18.5±0.39 MPa·mm$^{1/2}$ for $d$ =43–172 μm ($x$=0.05–0.5) and 35.7±1.3 MPa·mm$^{1/2}$ for $d$ =172–1,526 μm ($x$=0–0.05).

Obviously, grain size plays a key role in determining the mechanical performances of Mg-Nd-Zn-Zr alloys. Nevertheless, the effect of grain size on the fatigue behavior of this novel alloy system remains unclear. The present work tuned the grain size of a Mg-2.6Nd-0.35Zn-*x*Zr (wt.%) alloy by changing the content of Zr element, and investigated the effect of grain size on the fatigue behavior after heat treatment, an aspect previously overlooked but crucial for the engineering applications of the alloys[13-15]. The present work indicates that, in Mg-Nd-Zn-Zr alloys, a coarse-grained microstructure effectively suppresses fatigue crack propagation, while a fine-grained microstructure enhances resistance to crack initiation and extends the total fatigue life.

## 2 Experimental

The alloy with a nominal composition of Mg-2.6Nd-0.35Zn (wt.%) was prepared by melting pure Mg (99.96wt.%), Zn (99.95wt.%), and an Mg-25wt.%Nd master alloy. A Mg-33wt.%Zr master alloy served as the grain refiner. All starting materials were preheated at 250 °C for 1–2 h to remove moisture. The cast iron crucible was pre-treated with a dilute HCl solution for 30–40 min and then heated together with other tools at 200 °C for 0.5–2 h, followed by the application of a BN coating to its surface. Under a protective gas atmosphere, pure Mg ingots were firstly melted and heated to 730–750 °C, then, the Mg-25wt.%Nd intermediate alloys and the Zn ingots were put into a crucible and melted completely with stirring. After that, the Mg-33wt.%Zr grain refiner alloys were added together with the RJ5 agent consisted of (24–30)wt.% $MgCl_2$, (20–26)wt.% KCl, (28–31)wt.% $BaCl_2$, (13–15)wt.% $CaF_2$, and 8wt.% NaCl/$CaCl_2$. Finally, the melt was poured into a cylindrical mold cavity (10 mm in diameter and 80 mm in length) to produce the test specimens.

Coupled plasma-atomic emission spectrometry (ICP-AES, Thermo Fisher ICP-7400) was used to determine the Zr content of the samples. Approximately 20 g of surface scale (scurf) was removed from the samples by drilling and about 200 mg scurf was dissolved in 20 mL hydrochloric acid, with a concentration of 32%, for 24 h. Then the solutions were detected by the ICP-AES machine. Two kinds of samples with Zr contents of 0.12wt.% and 0.46wt.% were obtained, respectively.

The heat treatment process began with immersion of the samples in a chromate solution for approximately 15 min. The samples were then placed in a furnace containing a mixture of $Fe_2S$ and S to provide a protective atmosphere and prevent oxidation. Solution treatment was carried out at 525±5 °C for 8 h, followed by quenching in warm water (60–80 °C). Subsequently, aging was performed at 250±5 °C for approximately 14 h, followed by air cooling.

The metallographic samples were cut from the as-cast samples with sizes of 10 mm×10 mm×15 mm, and then successively ground and polished by #200, #400, #800, #1200 sand papers and 6 μm, 1 μm diamond paste. After that, the samples were etched using a corrosive solution composed of 4.2 g of trinitrophenols, 10 mL of acetic acid, 10 mL of $H_2O$, and 70 mL of alcohol. The metallography was observed by using Olympus PMG3 and Reichert-Jung Polyva optical microscopy. The grain size was calculated following the standard ASTM E112-88: Standard test methods for determining grain size[16]. The LSM 880 confocal laser scanning microscope was used to characterize the macroscopical three-dimensional morphology of the fracture surface after fatigue cracking using a 405 nm wavelength laser. The scanning sizes were 3,000.0 μm×2,546.5 μm for every point. Hitachi S-4700 and Hitachi S-570 scanning electronic microscopes were used to reveal the microstructures including the fatigue propagation paths and fracture surface, operated at an accelerating voltage of 15 kV, at 20.0 mA.

The tensile behavior was measured at room temperature on an Instron 5500R at a tensile rate of 1 mm·min$^{-1}$, with a sample geometry according to standard GB/T 228.1-2021: Metallic materials-Tensile testing, Part 1: Method of test at room temperature[17], as shown in Fig. 1(a). The fatigue behavior measurements were carried out at room temperature on an MTS 809 Axial/Torsional test system under the axial tensile and compress mode by referring the standard GB/T 6398-2017: Metallic materials-fatigue testing-fatigue crack growth method[18]. Sinuidal wave-like force loading was used in the measurements. The fatigue life tests were carried out on samples with geometry shown in Fig. 1(b). The stress ratio $R$ was 0.1 and the loading was adopted as 130, 120, 100, 80, 70 MPa, respectively. The stress-life ($S$-$N$) data of the samples were obtained under sinusoidal loading with a frequency of 10 Hz. The samples for fatigue crack propagation testing were machined into the geometries shown in Figs. 1(c) and (d). Loading force of 4 kN was applied to present the fatigue crack propagation process, under experimental frequencies of 2 Hz and 10 Hz. Loading force of 0.8 kN was used to probe the fatigue crack propagation threshold, under frequency of 10 Hz. The stress ratio was also 0.1. The applied loading force was selected based on conventional ranges for magnesium alloys: 0.1–1 kN

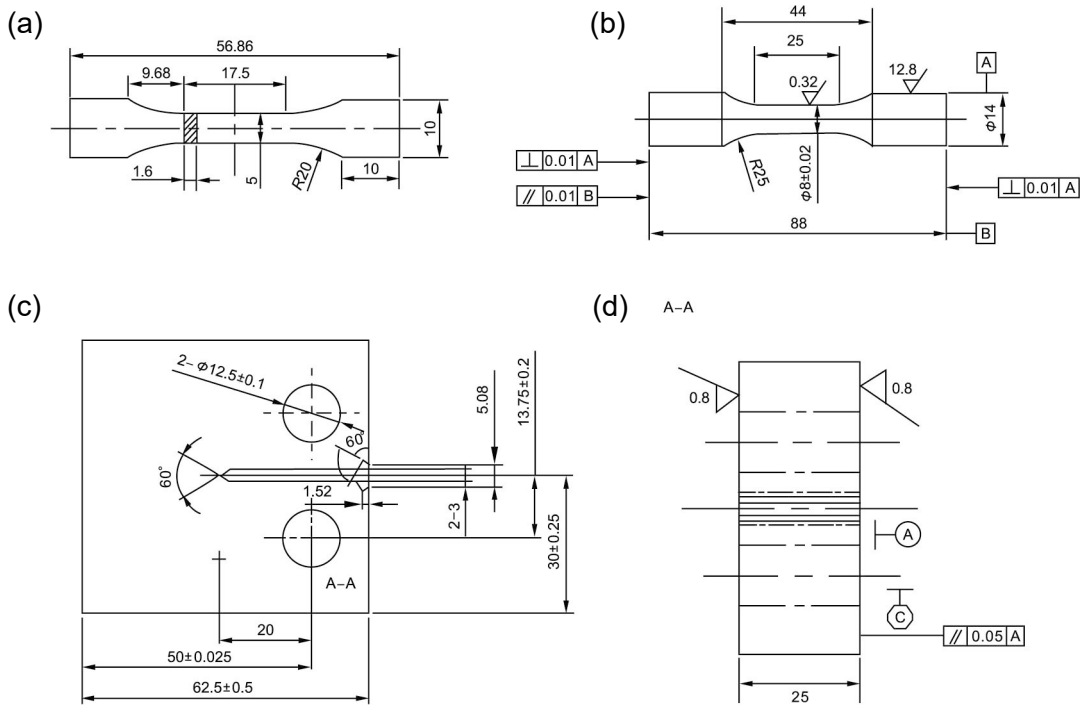


**Fig. 1: Sample geometry for mechanical properties measurements: (a) tensile behavior test; (b) fatigue life tests; (c) fatigue crack propagation test; (d) A–A section of (c) (Unit: mm)**

for fatigue testing in the threshold regime and 1–5 kN for the stable crack propagation regime[19]. The crack growth rate was calculated according to the test date by the MTS TestSuite™ Multipurpose software.

## 3 Results and discussion

The metallographic microstructures of the alloy with 0.12wt.% and 0.46wt.% Zr after heat treatment are shown in Fig. 2. The sample containing 0.12wt.% Zr [Fig. 2(a)] exhibits a significantly larger average grain size of 596 μm compared to that containing 0.46wt.% Zr [Fig. 2(b)], which has an average grain size of approximately 94 μm. It primarily consists of equiaxed grains with embedded dendritic structures. In contrast, the sample containing 0.46wt.% Zr predominantly features globular grains. These results demonstrate the excellent grain refinement efficiency of Zr addition in magnesium alloys[20-22]. Such grain refinement effect endows the samples with fine grains, resulting in much better tensile performances compared to that with coarser grains, as shown in Fig. 3. The tensile strength was measured as 244.6±8.8 MPa for the sample with a grain size of 94 μm and 184.5±7.7 MPa for the sample with a grain size of 596 μm, indicating that the finer-grained sample exhibits a 32.6% higher tensile strength. Similarly, the elongation is (9.18±2.2)% for the 94 μm grain sample, compared to (3.8±1.3)% for the 596 μm grain sample. The 0.2% offset yield strength is estimated to be approximately 128.8±3.6 MPa and 96.2±3.2 MPa for the 94 μm and 596 μm grain samples, respectively. These improved tensile performances hint a better fatigue property for the sample with smaller grains.

Fatigue life is a critical property to guarantee the fatigue design in practical engineering applications of materials. Figures 4(a) and (b) show the *S-N* data for samples with

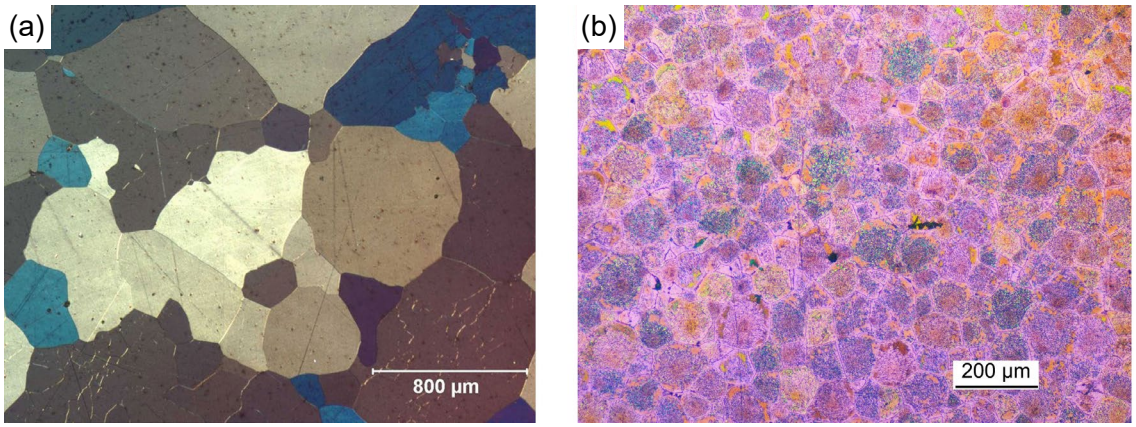


**Fig. 2: Metallographical microstructures of Mg-2.6Nd-0.35Zn-*x*Zr (wt.%) after heat treatment: (a) *x*=0.12; (b) *x*=0.46**

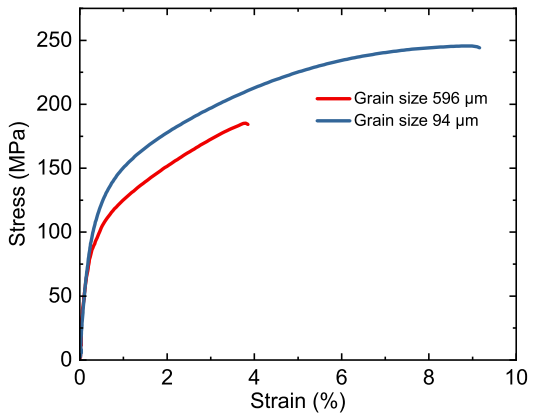


**Fig. 3: Tensile behaviors of samples containing 0.12wt.% (average grain size: 596 μm) and 0.46wt.% Zr (average grain size: 94 μm)**

grain sizes of 596 μm and 94 μm, respectively. Fatigue life significantly increases with decreasing stress for both samples. The effect of grain size on fatigue life is demonstrated by a longer fatigue life for the sample with finer grains. Under 130 MPa, the fatigue life reaches $N_f$=1.2×10$^4$ cycles for the 94 μm sample. However, it is only $N_f$=1.2×10$^3$ cycles for the 596 μm sample. These results are consistent with observations reported in previous studies of other alloys[23-25].

Regarding the *S-N* relationship, it can be observed that the fatigue life (number of cycles to failure) does not exhibit a linear dependence on applied stress amplitude. This behavior deviates from Miner's rule, which assumes that fatigue damage accumulates linearly with each stress cycle[26]. Such deviation is likely attributed to sequence effects[27]. The *S-N* data also exhibit significant scatter, with greater variability at lower

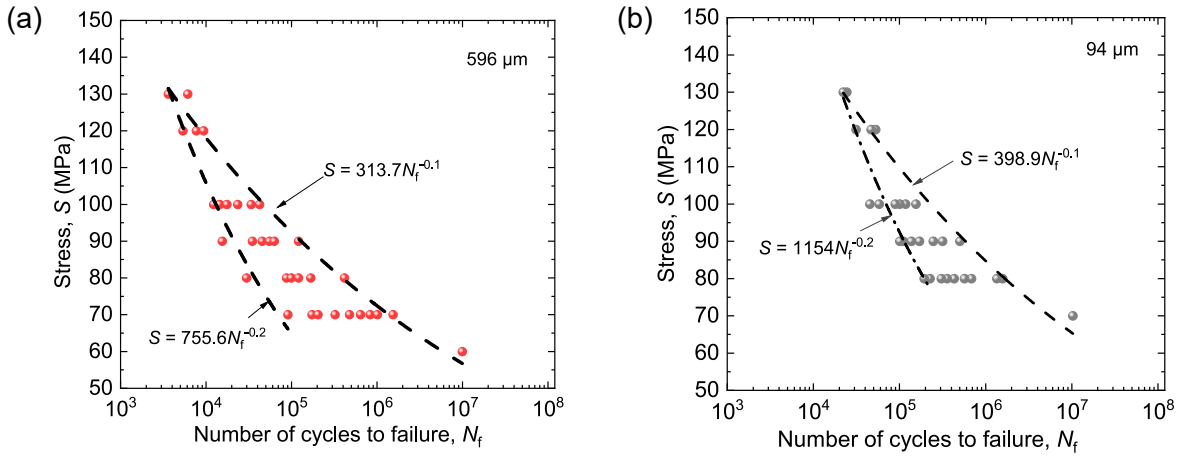


**Fig. 4: Stress-life (*S-N*) curves of samples with grain size of 596 μm (a) and 94 μm (b), respectively**

stress levels. This increased scattering is often attributed to the presence of non-uniformly sized defects and microstructural inhomogeneities in sample, which affect the repeatability of individual tests[28]. Additionally, poor alignment of the testing machine and specimens may contribute to the observed scatter. Despite differences in grain size, the distribution of *S-N* data appears similar across all samples. To analyze this similarity, the commonly used Basquin model was employed to formulate the *S-N* relationship[29], which was written as

$$S=S_0N_f^p \quad (1)$$

where $p$ is strongly material dependent and often known as the fatigue strength exponent or Basquin exponent, $S_0$ represents the fatigue strength coefficient.

This model provides a nonlinear fit to the *S-N* data, as shown in Figs. 4(a) and (b) for the experimental samples. Considering data scatter, two curves were fitted based on the lower and upper fringes of *N*, respectively. It is found that both samples exhibit the same exponents ($p$ values) for the lower and upper fringe fitting curves, $p$=−0.2 for the lower fringe and $p$=−0.1 for the upper fringe. However, the fatigue strength coefficient $S_0$ differs between the samples. The 94 μm sample exhibits a larger $S_0$, regardless of the lower or upper fringe, i.e. 1,154 and 398.9, compared to the 755.6 and 313.7 of the 596 μm sample. Exponent $p$ provides insight into how fatigue strength diminishes with cycles, characterizing the material's fatigue sensitivity, while $S_0$ represents the static strength and the stress level at immediate failure. Our results suggest that finer grains lead to higher static strength, which aligns with the Hall-Petch relationship. In fact, it has been shown for most metals that $S_0$ is approximately equal to the true fracture strength ($\sigma_f$)[24]. While, the fatigue strength exponent $p$ is not significantly affected by grain size. This indicates that the fatigue damage mechanism remains similar across the samples with different grain sizes[30] and the variation of fatigue life is primarily attributed to the grain size-dependent fracture strength effect. In addition, the fatigue strength is usually determined according to the *S-N* relationship by defining it as the stress at the desired number of cycles for the component's service life (often 10$^7$), from the viewpoint of engineering application. In that case, the upper boundary of fatigue strength is calculated as 62.59 MPa and lower boundary is 30.08 MPa for the 596 μm sample, by setting the $N_f$ as 10$^7$ in the fitting *S-N* curves. While, the upper boundary of fatigue strength is 79.59 MPa and lower boundary is 45.94 MPa for the 94 μm sample. Smaller grain sample exhibits larger fatigue strength.

To understand the fatigue damage mechanism, the crack propagation behavior was studied, as shown in Figs. 5(a) to (d) for the 596 μm sample and Figs. 5(e) to (h) for the 94 μm

sample. In the 596 μm sample, the crack exhibits a winding path, particularly at the early stages of propagation, indicating that the crack is disturbed and changes its propagation direction. Figures 5(a) and (b) show that the propagation direction undergoes an abrupt angular shift, suggesting crack propagation along grain boundaries, which is consistent with the intergranular fracture model. In contrast, for the 94 μm sample, the crack propagates almost straight [Fig. 5(e)] without significant directional changes [Fig. 5(f)], corresponding to a predominantly transgranular fracture mechanism [Fig. 5(g)]. This also explains why the 94 μm sample exhibits superior tensile strength, yield strength, and elongation compared to the 596 μm sample. Ahead of the crack tip, intensive slip bands are observed, resulting from stress concentration at the crack front [Figs. 5(c) and (h)]. In the 596 μm sample, the slip bands are of higher density, shorter length, and thinner thickness compared to those in the 94 μm sample. Additionally, in the coarse-grained (596 μm) sample, the slip bands appear in multiple directions, indicating the occurrence of multiple slip processes. In contrast, in the fine-grained (94 μm) sample, the slip bands are nearly parallel and align along a single direction within individual grains.

Figure 6 further illustrates the three-dimensional morphology of the fatigue fracture surface at macroscopical scale obtained from the fatigue crack propagation tests. In Figs. 6(a) and (g), the fracture surface of the alloys can be divided into two regions by the red line. The left region appears flatter than the right, which corresponds to the instantaneous fracture zone, while the right region represents the stable crack propagation zone. Such fracture characteristics are different from that observed in conventional fatigue fracture surfaces without notches at the initial crack propagation stage. In unnotched specimens, crack initiates at surface sites such as defects, inclusions, or grain boundaries due to the absence of stress concentration.

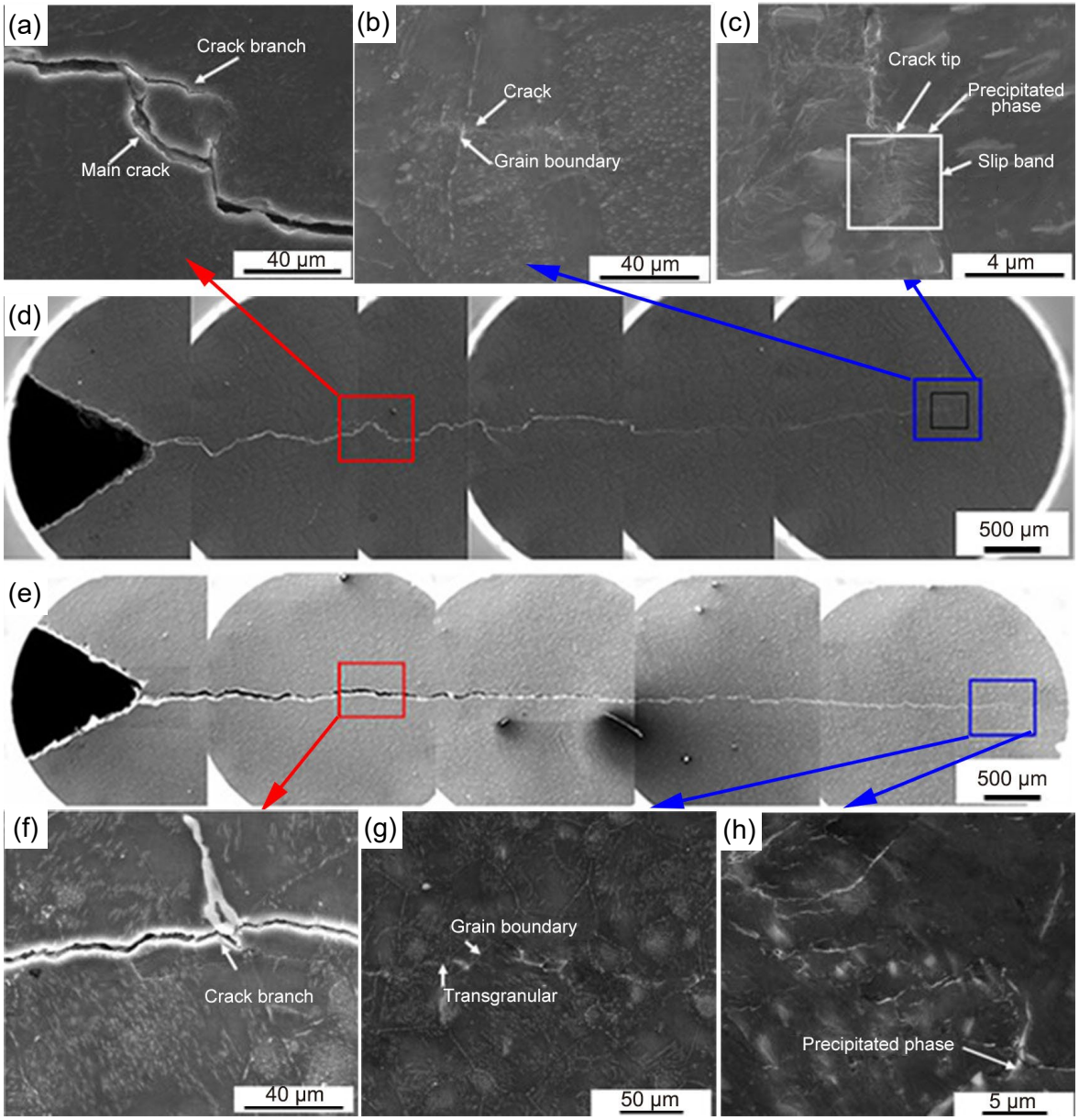


**Fig. 5: Fatigue crack propagation of samples with grain size of 596 μm (d) and 94 μm (e): (a)–(c) magnified images of the regions marked by boxes in (d); (f)–(h) magnified images in the regions marked by boxes in (e)**

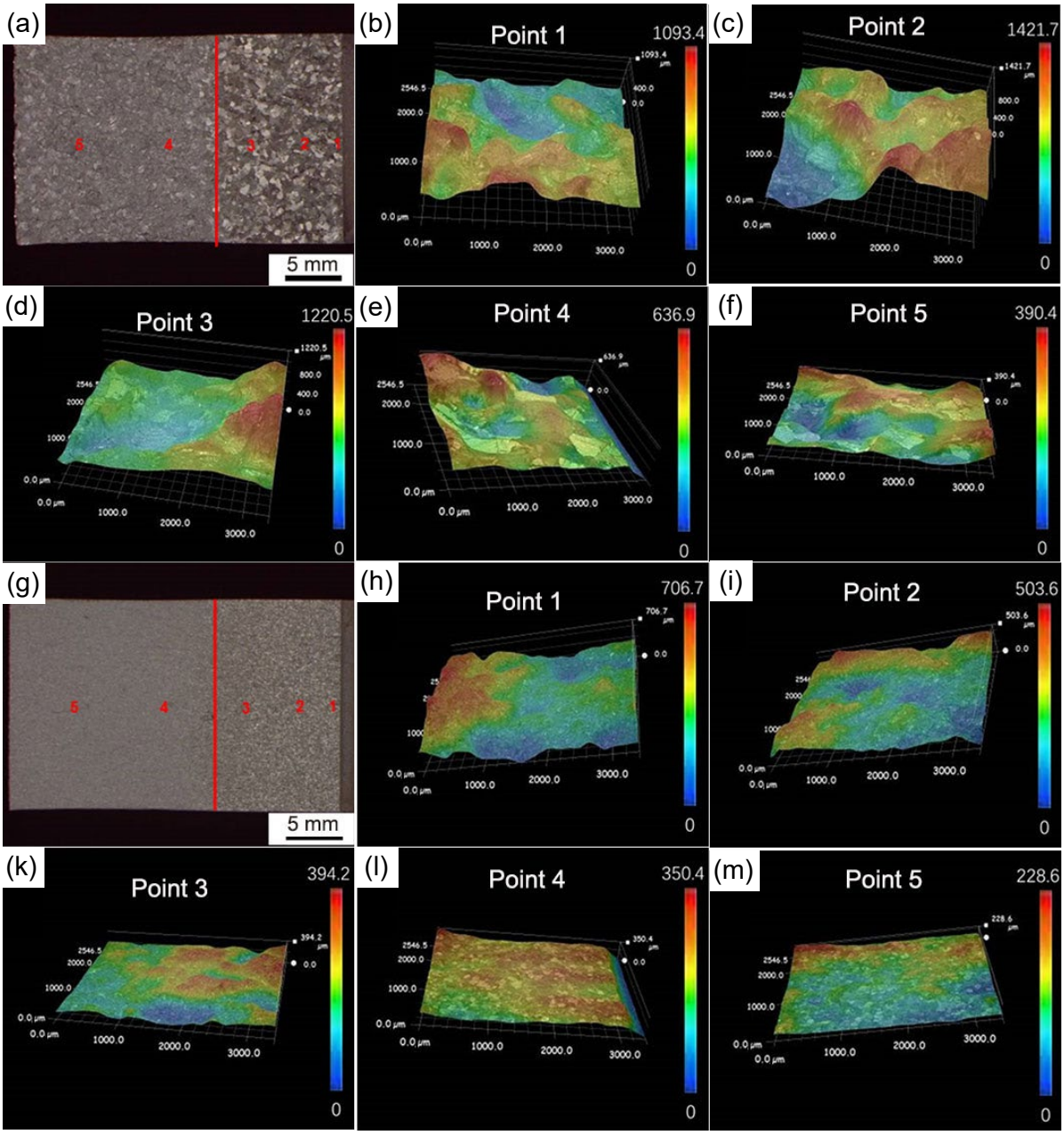


**Fig. 6: Metallographical macro-graphs of fatigue fracture surface (a, h) and the three-dimensional images at the selected points: (a–f) sample with grain size of 596 μm; (g–m) sample with grain size of 94 μm**

Consequently, persistent slip bands are commonly observed during the early stages of crack propagation. A certain of plastic deformation with high density of dislocations would be seen there[31]. In contrast, the local stress concentration associated notching would suppress the formation of slip bands and causes instantaneous crack initiation with brittle crack morphologies.

The fatigue fracture surface of the 596 μm samples is rougher than that of the 94 μm samples in both the instantaneous and stable fracture regions. This increased roughness could be attributed to the significantly larger grain size and intergranular fracture of the 596 μm samples. More specifically at microscopical scale, Fig. 7 presents the position-dependent crack surface micro-morphology of the 596 μm samples. Figures 7(a) to (c) show that the stable fracture region contains fatigue striations and some secondary cracks, as indicated by the blue arrows in Fig. 7(b). In contrast, the instantaneous fracture region exhibits cleaved planes and cleavage steps [Figs. 7(d)–(f)], indicative of a brittle fracture mode during the instantaneous fracture. The crack surface micro-morphology of the 94 μm samples differs from that of the 596 μm samples. In the stable fracture region, the crack surface displays a high density of fatigue striations and a low density of small secondary cracks [Figs. 8(a)–(c)], similar to the 596 μm samples. However, the spacing between the fatigue striations is wider than that observed in the 596 μm samples, suggesting a lower crack propagation rate in the larger-grained samples during the stable fracture stage. In the instantaneous fracture region, the crack surface of the 94 μm samples exhibits mixed features, including cleaved planes, tearing ridges, and dimples [Figs. 8(d)–(f)], indicating the presence of ductile fracture to some extent.

Theoretically, fatigue crack growth proceeds through three

stages. The first stage occurs in the near-threshold regime, where the crack propagation is very slow and highly sensitive to the microstructure. The second stage corresponds to the stable crack propagation stage, during which the influence of microstructure on sensitivity of crack propagation is reduced. The third stage is the instantaneous fracture stage[32]. Figure 9(a) presents the relationship between crack length and fatigue cycle number $N_f$ under a force of 4 kN and a frequency of 10 Hz. In fact, the curves do not clearly display the near-threshold regime at very low fatigue life ($N_f \approx 0$). A large portion of the curve corresponds to the stable propagation stage, where the crack length exhibits a weakly nonlinear dependence on the number of the loading cycles. A gradual acceleration of crack propagation is observed as $N_f$ increases. When $N_f$ approaches a critical limit, the crack length increases sharply, marking the instantaneous fracture stage. Notably, the crack length of the 94 μm samples is consistently longer than that of the 596 μm samples at the same fatigue cycle number, indicating that crack growth is more rapid in the 94 μm samples.

The stress intensity factor ($K$) represents the severity of stress distribution near the crack tip and can be calculated for the geometry of the fatigue crack growth test sample (Fig. 1) using the following model[33]:

$$K = \frac{F}{BW^{1/2}}\left[29.6\left(\frac{\alpha}{W}\right)^{1/2} - 195.5\left(\frac{\alpha}{W}\right)^{3/2} + 655.7\left(\frac{\alpha}{W}\right)^{5/2}\right] \quad (2)$$

where $F$ is the loading force, $B$ is sample thickness and $W$ is the sample width, $\alpha$ is the distance between the crack tip and the positioning hole. Figures 9(b) and (c) indicate the relationship between the fatigue crack growth rate and the stress intensity factor $K$ at different fatigue frequencies for the 596 μm samples and the 94 μm samples, respectively. Overall, the crack growth rate is not significantly affected by grain size in the present samples and increases with $K$. A higher fatigue frequency results in an increased crack growth rate. Moreover, when $K$ is smaller than approximately 9, the logarithm of the fatigue crack growth rate exhibits a linear dependence on log($K$), followed by a rapid increase beyond this threshold. The linear regime corresponds to the stable crack growth phase in theory and can be quantitatively described by the Paris equation[34]:

$$\frac{\mathrm{d}\alpha}{\mathrm{d}N_f} = CK^m \quad (3)$$

Thus, it is reasonable to see $\log(\mathrm{d}\alpha/\mathrm{d}N_f)=\log C+m\log K$,

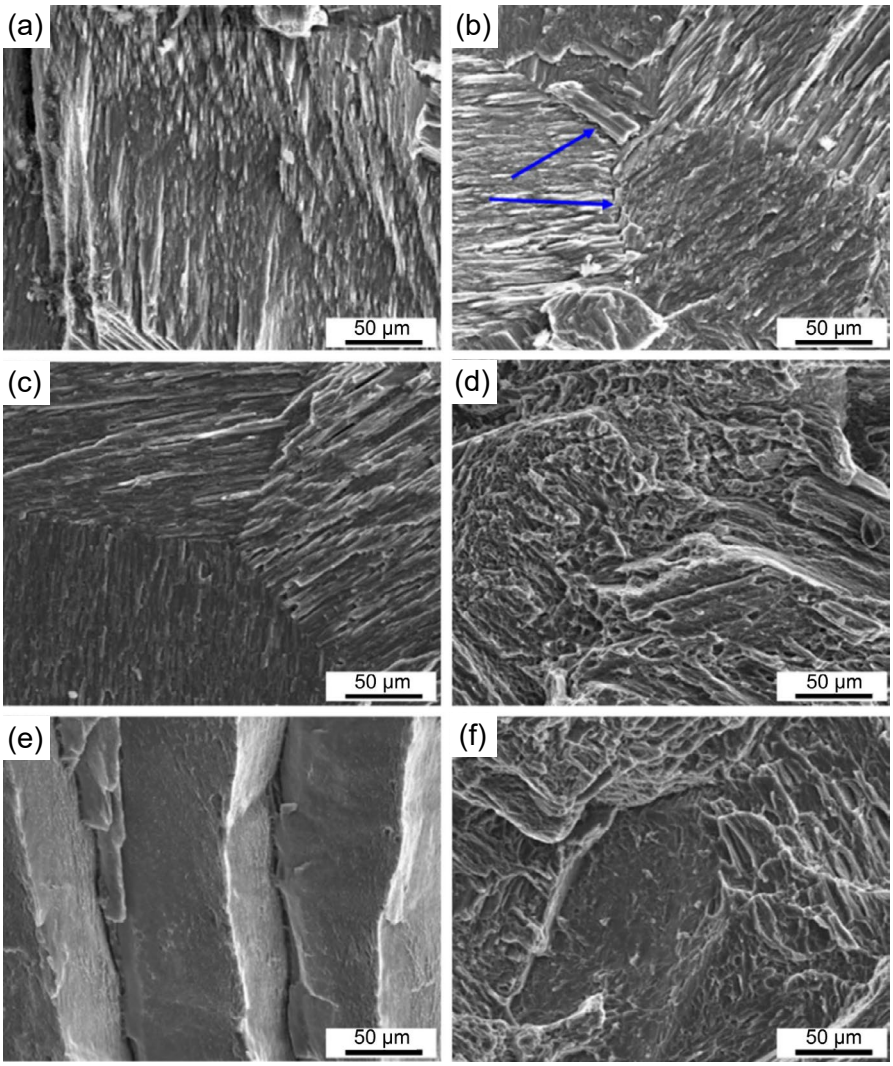


**Fig. 7: Fracture surface images of the 596 μm sample at positions depart from the crack tip 2 mm (a), 4 mm (b), 8 mm (c), 15 mm (d), 20 mm (e), 26 mm (f)**

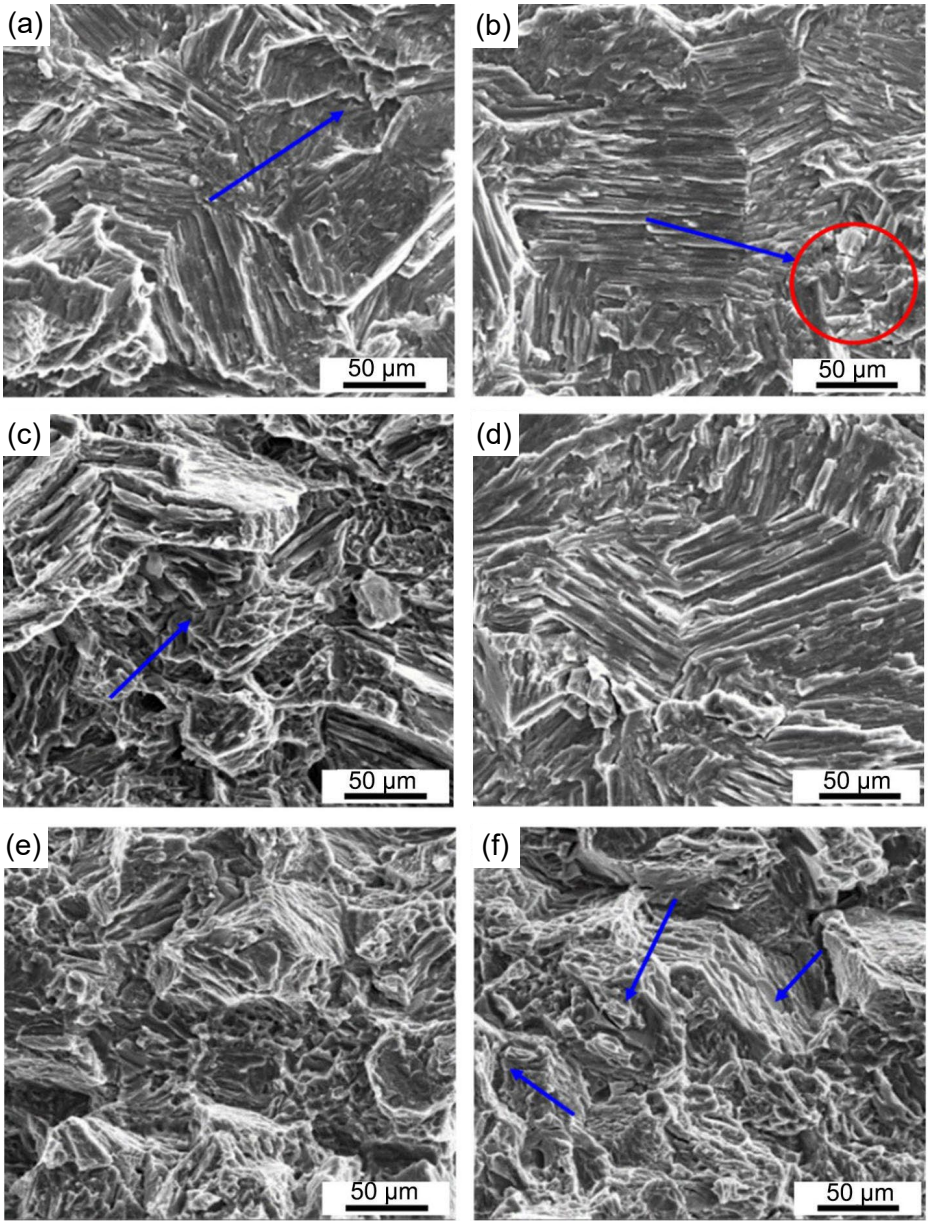


**Fig. 8: Fracture surface images of the 94 μm sample at positions depart from crack tip 2 mm (a), 4 mm (b), 8 mm (c), 15 mm (d), 20 mm (e), 26 mm (f)**

where $C$ and $m$ are constants determined by many factors such as materials composition and loading conditions, $N_f$ represents number of cycles to failure. The rapid increase in the regime marks the instantaneous fracture stage. The curves in Figs. 9(b) and (c) were fitted using Eq. (3) in the stable growth stages, enabling the determination of the parameters $C$ and $m$ for the samples at different frequencies, as shown in Table 1. Clearly, higher fatigue frequencies result in larger $C$ and $m$ values. For the investigated Mg-Nd-Zn-Zr alloys, finer grain sizes are associated with larger $m$ values. This finding is consistent with previous reports on other materials[35], indicating that the crack growth rate is more sensitive to the stress intensity factor in fine-grained samples. However, a definitive conclusion regarding the dependence of $C$ on grain size cannot be drawn, as it appears to vary with frequency.

Furthermore, the fatigue crack propagation threshold ($K_{th}$) for the two types of samples was determined by tests under a low force loading of 0.8 kN, as shown in Fig. 9(d). The results indicate that the threshold $K_{th}$ values for the 596 μm and 94 μm samples are 3.23 MPa·m$^{1/2}$ and 1.74 MPa·m$^{1/2}$, respectively. Additionally, the threshold $K_{th}$ can be evaluated using the following equations proposed by Estrin et al.[36]:

$$K_{th} \approx \sigma_y \sqrt{d} \quad (4)$$

or

$$K_{th} \cong \sigma_{fo} \sqrt{\pi d} \quad (5)$$

where $\sigma_y$ and $\sigma_{fo}$ are the cyclic yield stress and the stress at which the fatigue cycle number is $10^7$, $d$ represents the characteristic size of the "structural unit" responsible for fracture (here refers to grain size). The $\sigma_y$ can be approximate to the yield stress of material, i.e. 128.8±3.6 MPa for the 94 μm sample and 96.2±3.2 MPa for the 596 μm sample.

The $\sigma_{fo}$ is right the fatigue strength that obtained according to Fig. 4, which is 30.08–62.59 MPa for the 596 μm sample

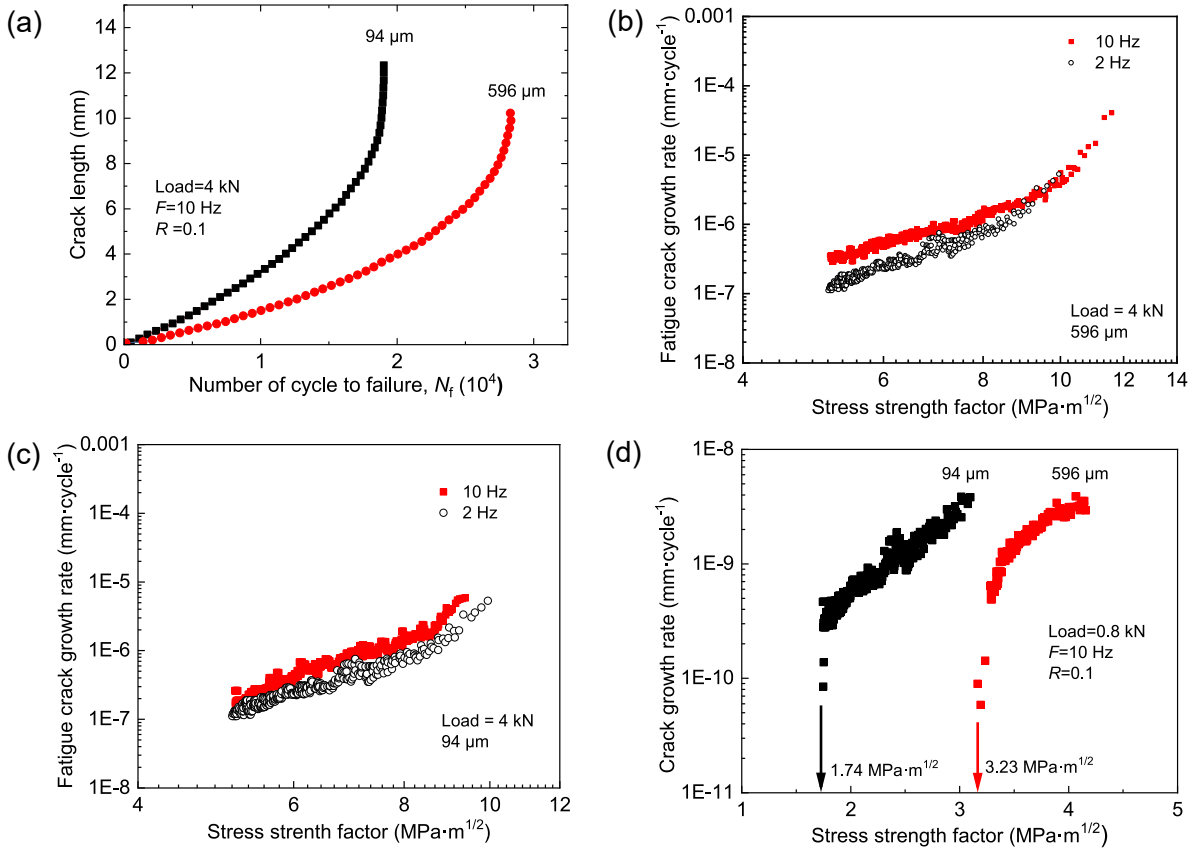


**Fig. 9: Fatigue performances of samples: (a) change of fatigue crack length as a function of fatigue cycle; (b)–(c) relationship between fatigue crack growth rate and stress intensity factor under different fatigue frequencies for the 596 and 94 μm samples, respectively; (d) threshold stress intensity factor of fatigue crack propagation for the two types of samples**

**Table 1: *m* values of alloys with different grain sizes at 2 Hz and 10 Hz**

| Grain size (μm) | *F* (Hz) | *C* | *m* |
|---|---|---|---|
| 94 | 2 | $1.62\times10^{-10}$ | 4.08 |
| 94 | 10 | $4.67\times10^{-10}$ | 5.02 |
| 596 | 2 | $1.72\times10^{-10}$ | 3.18 |
| 596 | 10 | $1.85\times10^{-10}$ | 4.0 |

and 45.94–79.59 MPa for the 94 μm sample. Accordingly, the $K_{th}$ was estimated via two approaches. According to Eq. (3), $K_{th}$ is approximately 2.34 MPa·m$^{1/2}$ for the coarse-grained sample (596 μm) and 1.24 MPa·m$^{1/2}$ for the fine-grained sample (94 μm). Alternatively, following the criterion in Eq. (4), $K_{th}$ ranges 1.30–2.70 MPa·m$^{1/2}$ and 0.78–1.36 MPa·m$^{1/2}$ for the 596 μm and 94 μm samples, respectively. The theoretical results present above are in reasonable agreement with the measured threshold values in Fig. 9(d): 3.23 MPa·m$^{1/2}$ for the 596 μm sample and 1.74 MPa·m$^{1/2}$ for the 94 μm sample. Thus, fine grains are associated with a lower fatigue crack propagation threshold in the Mg-Nd-Zn-Zr alloys investigated in this study, which is consistent with previous studies on other alloys. For instance, in high-strength low-alloy steels, the $K_{th}$ was found increasing as the grain size grew from 10 to 123 μm[37]. Recalling that crack growth is easier in fine-grained samples (94 μm), as discussed above, this can be attributed to their lower fatigue crack propagation threshold.

The above analysis presents the effect of grain size on crack growth behavior in Mg-Nd-Zn-Zr alloys. Fine grains lead to higher stress intensity factor sensitivity and a lower fatigue crack propagation threshold, resulting in reduced crack propagation resistance for the sample with a smaller grain size of 94 μm.

Thus, it has been demonstrated that, although the fine-grained Mg-Nd-Zn-Zr alloy exhibits lower crack growth resistance, it achieves a longer fatigue life. This observation is consistent with findings in many structural alloys, where crack growth resistance generally improves with increasing grain size, while the total fatigue life, as measured by *S-N* plots, shows the opposite trend[27]. This apparent contradiction is often explained by the fact that crack growth resistance is measured on a sample with a pre-existing flaw, whereas the *S-N* test is conducted on a flaw-free sample. As a result, the total fatigue life consists of both the crack initiation life and the crack growth life to failure. Based on this, it can be concluded that the fine-grained sample exhibits better crack initiation resistance in the Mg-Nd-Zn-Zr alloys in this study. A similar trend has been observed in a nickel-based superalloy, where the proportion of crack initiation life in the total fatigue life increased as grain size decreased, leading to an overall increase in fatigue life due to the prolonged crack initiation life[38].

Crack initiation is often thought to occur along persistent slip bands (PSBs) within grains, as strain gradients change abruptly at the interface between the PSBs and the matrix[39, 40]. Furthermore, PSBs are favored to form in coarse grain materials[39, 41, 42] due to the easier accommodation of strain through multiple slip processes in coarse grains. In contrast, the higher initial dislocation density in fine grains reduces the ability to form PSBs[39]. At the early stages of deformation, slip sources on opposite sides of a coarse grain can be independently activated as the grain size exceeds the interaction length of the slip sources. As a result, multiple slip processes occur more readily in coarse grains. In fine-grained samples, however, the stress field due to deformation encompasses the entire grain, leading to a single slip process. These behaviors are evident in our samples, as shown in Figs. 5(d) and (e).

Regarding crack propagation resistance, coarse grains are more effective in activating crack deflection or branching. This occurs because grain boundaries and changes in crystal orientation can shield the crack tip from stress, thereby slowing down the development of PSBs and retarding crack propagation[27]. In such cases, a tortuous crack path forms, favoring an intergranular fracture mode. This behavior is evident in the present study. As shown in Fig. 5, the crack propagation path in the coarse-grained sample (596 μm) exhibits significant directional changes with large deflection angles, following the grain boundaries. In contrast, the crack propagation path in the fine-grained sample (94 μm ) is much straighter and smoother.

# 4 Conclusions

The fatigue behavior of cast Mg-2.6Nd-0.35Zn-*x*Zr (wt.%) alloy samples with varying grain sizes was investigated. Following results are achieved:

(1) Grain size significantly affects fatigue crack propagation. The fine-grained sample exhibits a straighter, smoother crack propagation path, indicative of a transgranular-dominated propagation mode. In contrast, the coarse-grained sample shows predominantly intergranular crack propagation, with frequent changes in crack direction along grain boundaries.

(2) The fatigue fracture surface of the coarse-grained sample shows a high density of cleaved planes, while the fine-grained sample displays a mixed morphology with tearing ridges, dimples, and fewer cleaved planes in the final instantaneous break stage.

(3) Quantitative analysis reveals that the crack tip in the fine-grained sample is more sensitive to stress concentration, as indicated by a larger stress intensity factor compared to the coarser-grained sample.

(4) Mg-2.6Nd-0.35Zn-*x*Zr alloys with larger grain sizes offer greater resistance to crack propagation, while fine-grained samples demonstrate longer total fatigue life due to their higher crack initiation resistance. Our results highlight the importance of optimizing grain size to maximize fatigue resistance in Mg-Nd-Zn-Zr alloys for engineering applications.

# Conflict of interest

The authors declare that they have no conflict of interest.

# References

[1] Pan H C, Ren Y P, Fu H, et al. Recent developments in rare-earth free wrought magnesium alloys having high strength: A review. Journal of Alloys and Compounds, 2016, 663: 321–331.
[2] Siemionek E, Majerski K, Surdacki P, et al. Review of magnesium alloys used in the manufacture of wheels for light vehicles. Advances in Science and Technology Research Journal, 2023, 17(6): 245–253.
[3] Chen J X, Tan L L, Yu X M, et al. Mechanical properties of magnesium alloys for medical application: A review. Journal of the Mechanical Behavior of Biomedical Materials, 2018, 87: 68–79.
[4] Prasad S V S, Prasad S B, Verma K, et al. The role and significance of magnesium in modern day research – A review. Journal of Magnesium and Alloys, 2022, 10(1): 1–61.
[5] Xie H, Zhao H, Guo X, et al. Recent progress on cast magnesium alloy and components. Journal of Materials Science, 2024, 59(22): 9969–10002.
[6] Fu P H, Peng L M, Jiang H Y, et al. Effects of heat treatments on the microstructures and mechanical properties of Mg-3Nd-0.2Zn-0.4Zr (wt.%) alloy. Materials Science and Engineering: A, 2008, 486(1): 183–192.
[7] Zhang X, Yuan G, Mao L, et al. Biocorrosion properties of as-extruded Mg-Nd-Zn-Zr alloy compared with commercial AZ31 and WE43 alloys. Materials Letters, 2012, 66(1): 209–211.
[8] Zhang T, Zhao X, Liu J, et al. The microstructure, fracture mechanism and their correlation with the mechanical properties of as-cast Mg-Nd-Zn-Zr alloy under the effect of cooling rate. Materials Science and Engineering: A, 2021, 801: 140382.
[9] Li Z, Fu P, Peng L, et al. Strengthening mechanisms in solution treated Mg-*y*Nd-*z*Zn-*x*Zr alloy. Journal of Materials Science, 2013, 48(18): 6367–6376.
[10] Karakulak E. A review: Past, present and future of grain refining of magnesium castings. Journal of Magnesium and Alloys, 2019, 7(3): 355–369.
[11] Ma Q, Das A. Grain refinement of magnesium alloys by zirconium: Formation of equiaxed grains. Scripta Materialia, 2006, 54(5): 881–886.
[12] Li Z M, Luo A A, Wang Q G, et al. Effects of grain size and heat treatment on the tensile properties of Mg-3Nd-0.2Zn (wt.%) magnesium alloys. Materials Science and Engineering: A, 2013, 564: 450–460.
[13] Hazeli K, Askari H, Cuadra J, et al. Microstructure-sensitive investigation of magnesium alloy fatigue. International Journal of Plasticity, 2015, 68: 55–76.
[14] Li X, Xiong S M, Guo Z, et al. Failure behavior of high pressure die casting AZ91D magnesium alloy. Materials Science and Engineering: A, 2016, 672: 216–225.
[15] Rettberg L H, Jordon J B, Horstemeyer M F, et al. Low-cycle fatigue behavior of die-cast Mg alloys AZ91 and AM60. Metallurgical and Materials Transactions: A, 2012, 43(7): 2260–2274.
[16] Standard ASTM E112-88: Standard test methods for determining grain size. American Society for Testing and Materials, Philadelphia, Pa, USA, 1988.
[17] Standard GB/T 228.1-2021: Metallic materials – Tensile testing, Part 1: Method of test at room temperature. National Standardization Administration of China and the State Administraion for Market Regulation, Issued on Dec. 2021.

[18] Standard GB/T 6398-2017: Metallic materials – Fatigue testing – Fatigue crack growth method. National Standardization Administration of China and the State Administraion for Market Regulation, Issued on July 2017.
[19] Ogarevic V V, Stephens R I. Fatigue of magnesium alloys. Annual Review of Materials Science, 1990, 20(20): 141–177.
[20] Liu Y, Zeng G, Liu H, et al. Grain refinement mechanism and research progress of magnesium alloy incorporating Zr. Acta Metallurgica Sinica, 2024, 60(2): 129–142.
[21] Sun M, Yang D, Zhang Y, et al. Recent advances in the grain refinement effects of Zr on Mg alloys: A review. Metals, 2022, 12(8): 1388.
[22] Sun M, Easton M A, StJohn D H, et al. Grain refinement of magnesium alloys by Mg-Zr master alloys: The role of alloy chemistry and Zr particle number density. Advanced Engineering Materials, 2013, 15(5): 373–378.
[23] Hoeppner D W, Grosskreutz J C. The effect of grain size on fatigue crack propagation in copper. In: Fatigue crack propagation, 1967, ASTM International. https://doi.org/10.1520/STP47240S
[24] Morrison D J, Moosbrugger J C. Effects of grain size on cyclic plasticity and fatigue crack initiation in nickel. International Journal of Fatigue, 1997, 19(93): 51–59.
[25] Liang F L, Laird C. Control of intergranular fatigue cracking by slip homogeneity in copper. I: Effect of grain size. Materials Science and Engineering: A, 1989, 117: 95–102.
[26] Miner M A. Cumulative damage in fatigue. In: Weibull W, Odqvist F K G (eds.). Colloquium on fatigue. IUTAM Symposia, 1945, Springer, Berlin, Heidelberg. https://doi.org/10.1007/978-3-642-99854-6_35.
[27] Suresh S. Fatigue of materials. Fatigue & Fracture of Engineering Materials & Structures, Cambridge University Press, 1991. https://doi.org/10.1017/CBO9780511806575.
[28] Murakami Y, Takagi T, Wada K, et al. Essential structure of SN curve: Prediction of fatigue life and fatigue limit of defective materials and nature of scatter. International Journal of Fatigue, 2021, 146: 106138.
[29] Basquin O. The exponential law of endurance tests. In: Proceedings of the American Society of Testing of Materials, 1910.
[30] Kun F, Carmona H A, Andrade J S, et al. Universality behind Basquin's law of fatigue. Physical Review Letters, 2008, 100(9): 094301.
[31] Sangid M D. The physics of fatigue crack initiation. International Journal of Fatigue, 2013, 57: 58–72.
[32] González-Velázquez J L. Fatigue fracture. In: Fractography and failure analysis, (ed. González-Velázquez J L), Cham., Springer International Publishing, 2018: 71–95.
[33] Anon: Stress intensity factors of cracks. In: Fatigue of structures and materials, (ed. Schijve J), Dordrecht, Springer Netherlands, 2009: 105–140.
[34] Paris P C, Erdogan F. A critical analysis of crack propagation laws. Journal of Basic Engineering, 1963, 85: 528–533.
[35] Li L, Zhang Z, Shen G. The effect of grain size on fatigue crack propagation in commercial pure titanium investigated by acoustic emission. Journal of Materials Engineering and Performance, 2015, 24(7): 2720–2729.
[36] Estrin Y, Vinogradov A. Fatigue behaviour of light alloys with ultrafine grain structure produced by severe plastic deformation: An overview. International Journal of Fatigue, 2010, 32(6): 898–907.
[37] Lucas J P, Gerberich W W. Low temperature and grain size effects on threshold and fatigue crack propagation in a high strength low alloy steel. Materials Science and Engineering, 1981, 51: 203–212.
[38] Zhu X, Gong C, Jia Y F, et al. Influence of grain size on the small fatigue crack initiation and propagation behaviors of a nickel-based superalloy at 650 °C. Journal of Materials Science & Technology, 2019, 35(8): 1607–1617.
[39] Keller R, Zielinski W, Gerberich W W. On the onset of low-energy dislocation substructures in fatigue: Grain size effects. Materials Science and Engineering: A, 1989, 113: 267–280.
[40] Lin M R, Fine M E, Mura T. Fatigue crack initiation on slip bands: Theory and experiment. Acta Metallurgica, 1986, 34(4): 619–628.
[41] Buque C, Bretschneider J, Schwab A, et al. Effect of grain size and deformation temperature on the dislocation structure in cyclically deformed polycrystalline nickel. Materials Science and Engineering: A, 2001, 319–321: 631–636.
[42] Weidner A, Beyer R, Blochwitz C, et al. Slip activity of persistent slip bands in polycrystalline nickel. Materials Science and Engineering: A, 2006, 435–436: 540–546.